NASA Technical Memorandum 101482

Finite Element Applications to Explore the Effects of Partial Bonding on Metal Matrix Composite Properties

J.J. Caruso
Lewis Research Center
Cleveland, Ohio

D. Trowbridge
University of Akron
Akron, Ohio

and

C.C. Chamis
Lewis Research Center
Cleveland, Ohio

Prepared for the
30th Structures, Structural Dynamics and Materials Conference
cosponsored by the AIAA, ASME, ASCE, AHS, and ACS
Mobile, Alabama, April 3–5, 1989

NASA

FINITE ELEMENT APPLICATIONS TO EXPLORE THE EFFECTS OF PARTIAL BONDING ON METAL MATRIX COMPOSITE PROPERTIES

J.J. Caruso
National Aeronautics and Space Administration
Lewis Research Center
Cleveland, Ohio 44135

D. Trowbridge
The University of Akron
Akron, Ohio 44325

and

C.C. Chamis
National Aeronautics and Space Administration
Lewis Research Center
Cleveland, Ohio 44135

E-4610

Abstract

The mechanics of materials approach (definition of E, G, ν, and α) and the finite element method are used to explore the effects of partial bonding and fiber fracture on the behavior of high temperature metal matrix composites. Composite ply properties are calculated for various degrees of disbonding to evaluate the sensitivity of these properties to the presence of fiber/matrix disbonding and fiber fracture. The mechanics of materials approach allows for the determination of the basic ply material properties needed for design/analysis of composites. The finite element method provides the necessary structural response (forces and displacements) for the mechanics of materials equations. Results show that disbonding of fractured fibers affect only $E_{\ell_{11}}$ and $\alpha_{\ell_{11}}$ significantly.

Nomenclature

A	area
E	Young's Modulus
e	effective value
F	force
f,m,ℓ	fiber, matrix, ply
G	shear modulus
S	physical dimension of the model
t	temperature
u,v,w	displacement in 1, 2, 3, direction
X,Y,Z	global coordinate axis system
α	thermal expansion coefficient
ε	strain
ν	Poisson's ratio
σ	stress
1,2,3	Laminate coordinate axis system

with finite element analysis to determine the behavior of epoxy matrix composites.[1] This method has been extended to high temperature metal matrix composites.[2]

The finite element method is not intended to replace experiments; but, to provide needed information not yet available through experiments. The finite element method provides a means to computationally simulate a physical experiment to estimate quantities which are difficult, or impossible, to menasure.

The objective of this work is to study the influence of disbonding of fractured fibers on the ply properties of metal matrix composites. In the study the disbonded fiber is considered fractured and therefore the load transfer between the fiber and matrix is inhibited by the amount of disbonding.

Modeling

The composite system considered for this work is P100-Graphite/Copper at 0.466 fiber volume ratio. Analyses for high temperature and room temperature ply material properties are conducted using Version 65 of MSC/NASTRAN.

A useful analytical tool in the evaluation of structures with repeated geometry is finite element analysis using the superelement method.[3] This involves the partitioning of a finite element mesh into separate collections of elements called superelements. Each superelement is solved separately and then combined to complete the analysis.

The composite superelement mesh is of modular nature, consisting of a unit cell (Fig. 1) and images of the unit cell; therefore, discontinuities can easily be added by substituting a conventional mesh, which models the discontinuity, in place of one of the images. This conventional mesh can also be imaged to simulate multiple discontinuities within the composite material. Some discontinuities of interest that can be modeled in this manner are partial bonding and fiber fracture, both common in metal matrix composite materials.

The cases chosen are but a few of a multitude of possible partial bonding configurations.

However, the cases selected are sufficient to understand the effects of partial bonding on the composite's material properties.

The mesh that is employed in this work consisted of a cluster of nine fibers in a three by three matrix (Fig. 2). The initial version of the mesh is assembled with the center fiber/matrix block modeled as a primary superelement and all surrounding blocks are images of the primary. This mesh is used when no fibers are disbonded and when all nine fibers are simultaneously disbonded. The mesh is reassembled when only the center fiber of the nine cell model is disbonded. For this case, the center block is modeled using conventional finite elements. The primary superelement is defined to be to one side of the center fiber and the remaining perimeter superelements are modeled as images of this one. Minor modifications are made to each of the meshes to allow for the modeling of varied amounts of disbond between fiber and matrix.

The approach used to simulate the disbond is described briefly here. Duplicate grid points are defined for all grids around the circumference of the fiber, at the interface between fiber and matrix. This duplicate grid point is included in the analysis only when the portion of fiber where it resided is to be disbonded from the matrix. The disbonding took place when the connectivity cards that define the perimeter of the fiber are altered so that one of the duplicate grids is associated with the fiber, and one with the matrix. No connectivity then exists across the interface of constituents, in effect producing a crack of zero width, with fiber on one side and matrix on the other. In the work described here, the total circumference of a fiber is released together. The amount of disbond is varied by disbonding different lengths of fiber as described above. For example, 2.78 percent disbonding of the center fiber is detailed in Fig. 3 with the plane of symmetry where the grids are not disbonded. No attempt is made to find the loading at which the disbonding or fiber fracture will take place or to prevent the overlapping of the fiber and the matrix after disbonding occurred. Instead, interest is placed on the effect of disbonding of the fractured fiber on the composite's material properties.

Procedure

The following are the procedures used to calculate ply material properties from the finite element output. The subscripts "11" are used to denote the direction along the fiber (longitudinal) and the subscripts "22" and "33" are used to denote the directions transverse to the fiber.

$\nu_{\ell 13}$, $\nu_{\ell 12}$, and $E_{\ell 11}$ are obtained from the same loading conditions. In this case the front face is fixed in the X($u_1 = 0.0$) and the back face is displaced in the X($u_9 = u$) (Fig. 2).

$E_{\ell 11}$ is calculated by finding the total force over the displaced face and dividing this force by the area of this face yielding an equivalent applied stress. The strain is then calculated by dividing the applied displacement by the length of the specimen. Young's modulus is computed from the mechanics of materials equation in the longitudinal 11 direction by:

INTRODUCTION

Recent research at NASA Lewis has led to the development of a computational method to predict the behavior of unidirectional composites. The method utilizes a mechanics of materials approach

$$E_{\ell 11} = \frac{\sigma^e_{\ell 11}}{\varepsilon_{\ell 11}} = \frac{F_{11} * s_1}{A_1 * u} \qquad (1)$$

where s_1 is the length in the 11 direction.

$\nu_{\ell 12}$ is found by finding the average deflection in the Y direction as a result of the enforced displacement in the X. Dividing this deflection by the width of the model yields a strain in the transverse direction (22). The Poisson's ratio $\nu_{\ell 12}$ is calculated from:

$$\nu_{\ell 12} = - \frac{\varepsilon_{\ell 22}}{\varepsilon_{\ell 11}} \qquad (2)$$

$\nu_{\ell 13}$ is found by similar methods.

To calculate the Poisson's ratio $\nu_{\ell 23}$ and the transverse modulus $E_{\ell 22}$, the face with the negative Y direction as its normal is fixed in the Y direction ($v_a = 0.0$) and the face with the positive Y direction as its normal has an enforced displacement in the positive Y direction ($v_g = v$) resulting in tension transverse to the fiber direction (Fig. 2). The equivalent applied stress is then calculated by averaging the resultant forces over the face and dividing by the face's area. $E_{\ell 22}$ and $\nu_{\ell 23}$ are calculated similarly to $E_{\ell 11}$ and $\nu_{\ell 12}$ respectively.

$E_{\ell 33}$ and $\nu_{\ell 32}$ are calculated from another unique set of boundary conditions in the same way $E_{\ell 22}$ and $\nu_{\ell 23}$ are calculated.

For the determination of $G_{\ell 21}$, an enforced displacement in the X direction is placed on the face with the positive Y axis as its normal. The shear strain is then calculated by dividing this displacement by the width of the model. The effective shear stress in the 21 direction is then calculated by dividing this force by the area over which it is applied. The shear strain for small displacements is given by the enforced deflection divided by the width of the specimen. $G_{\ell 21}$ is obtained by dividing the shear stress in the 21 direction by the shear strain.

$$G_{\ell 21} = \frac{\sigma^e_{\ell 21}}{\varepsilon_{\ell 21}} \qquad (3)$$

$G_{\ell 31}$ is found by similar methods from another unique set of boundary conditions.

$G_{\ell 23}$ can be obtained by applying an enforced displacement in the positive Z direction to the side whose normal is the positive Y axis. The total resulting force on this face is calculated from the finite element output. This total shear force in the 23 direction is divided by the area of the side over which it is applied, resulting in the average shear stress in the 23 direction. The small displacement shear strain in the 23 is then calculated by dividing the applied displacement in the Z direction by the width of the model. $G_{\ell 23}$ is calculated by dividing the effective shear stress, $\sigma^e_{\ell 23}$, by $\varepsilon_{\ell 23}$.

In order to calculate the thermal expansion coefficients $\alpha_{\ell 11}$, $\alpha_{\ell 22}$, and $\alpha_{\ell 33}$, a plane in the center of the model, with the positive X direction acting as its normal, is restricted from movement in the X direction ($u_5 = 0.0$). This restriction assures symmetry about the center of the model. A thermal load is then applied to the model, $T = T_o$.

The first step in finding $\alpha_{\ell 11}$ is determining the average of the displacements on the end with the positive X axis as its normal and dividing by the length of the model, s_1, resulting in the strain in the 11 due to the change in temperature. Now, by dividing the strain by the change in temperature, one can obtain the thermal expansion coefficient in the 11 direction.

$$\alpha_{\ell 11} = \frac{\varepsilon_{\ell 11}}{\nabla T} \qquad (4)$$

$\alpha_{\ell 22}$ is found by taking the average displacement in the Y direction and dividing by the change in temperature and the width.

The calculation of $\alpha_{\ell 33}$ is similar to that of $\alpha_{\ell 22}$, with the exception being that the average displacement in the Z is divided by the change in temperature and by the height of the model.

A set of reference finite element runs for P100/copper are executed with a 0.466 fiber volume ratio. These runs contained no disbonding or fiber fracture. Composite ply material properties are calculated from the output of these finite element runs (Table I). Additional confidence was gained by comparing the ply properties in Table I with those predicted by Caruso and Chamis[2] and by Hopkins and Chamis[4] with very good correlation.

Disbonding and fiber fracture of a single fiber in the center of the nine cell model is now considered (Fig 3). Room temperature (70 °F) material properties are used (Table II). In all loading conditions, fibers that are to be disbonded are also considered fractured and; therefore, did not have an applied displacement assigned to them. This modeled the fiber fracture in advance of disbonding. In this first series of runs, each element around the circumference of the fiber is allowed to disbond using the methods described earlier. The disbonding of a fractured fiber is done for each successive layer of elements along the length of the fiber. After the mesh is changed to reflect the next layer of disbonding, the loading conditions are applied and ply material properties calculated. Results are plotted for each of the ply material properties verses percent disbond of the total mesh (Figs. 4 to 7). These plots show the properties affected most by disbonding and to what degree they are affected. Some of these properties can be used as indicators of partial bonding of a fractured fiber in cases where material properties are not near predicted values. When suspecting the presence of partial bonding, closer attention should be paid to those properties found to be more sensitive to the presence of the fiber disbonding.

The next series of runs are executed with high temperature constituent material properties (Table II). The temperature selected is 1500 °F. The results of the material property calculations are shown in Figs. 8 to 11. Note that these plots reflect a little over 11 percent disbonding of the entire composite. This is a result of releasing only the center fiber for these cases considered here. The 11 percent disbonding value shown on these plots represents the point at which the center fiber is totally disbonded and the surrounding eight fibers are fully bonded to the matrix. When the fractured center fiber is considered completely disbonded it is still connected to the matrix material by a ring of nodes in the plane of symmetry (Fig 3). This can add some stiffness transversely and in shear.

The next series of conditions considered are when all nine fibers in the model are disbonded and the room temperature boundary conditions are imposed. In this case the percent disbonding can go up to 100 percent of the total fiber length. Once again, the connectivity of a ring of nodes in the plane of symmetry around each fiber is maintained at 100 percent disbonding. Material properties are calculated by applying each of the loading conditions described earlier. These results are plotted showing the effect of fiber disbonding on each property when all fibers are equally disbonded (Figs. 12 to 15).

The next series of runs is repeated for high temperature conditions. All nine fibers are released as described above using material properties that reflected a use temperature of 1500 °F. Material properties are calculated and plotted for varying degrees of fiber disbonding ranging from 0 to 100 percent disbonding (Figs. 16 to 19).

Results and Discussion

The degradation in the ply material properties could be influenced by the difference in the corresponding fiber and matrix material properties. As the fibers become structurally inactive, the matrix material properties have a more significant role in determining the composite's global properties. Ideally, the composite's material properties are bounded by the highest and lowest values of its constituents; however, it will be seen that a composite ply material property can be lower than the lowest constituent property.

Room Temperature Ply Properties with Center Fiber Disbonding

Figure 4 shows the degradation of the modulus in the 11, 22 and 33 directions due to disbonding of the center fiber only. These results reveal that the longitudinal modulus has decreased by about 8 percent while disbonding is at 11.1 percent of the total circumferential fiber area of the model.

The percent decrease in $E_{\ell 22}$ and $E_{\ell 33}$ for 11.1 percent total fiber area disbonding is 1.5 percent. From these results it can be concluded that $E_{\ell 11}$ is more sensitive to fiber disbonding than the transverse moduli. The decrease in $E_{\ell 11}$ is due mostly to geometric effect. The geometric effect is the holes left behind by the

disbonded fiber much like a sponge. From further results it will become evident that $E_{\ell 11}$ is the second most sensitive property to fiber disbonding.

The effect of fiber disbonding on Poisson's ratio for center fiber disbonding is depicted in Fig. 5. When the center fiber is completely disbonded (11.1 percent total fiber length disbonding), $\nu_{\ell 12}$ and $\nu_{\ell 13}$ have degraded by 0.5 percent. A decrease of 1.6 percent in $\nu_{\ell 23}$ and $\nu_{\ell 32}$ is witnessed when total center fiber disbonding is achieved. This degradation of Poisson's ratio is very small and can be considered insignificant.

The decrease in shear modulus due to center fiber disbonding is shown in Fig. 6. The percent change in $G_{\ell 12}$ is 3 percent and $G_{\ell 23}$ is 2 percent when the center fiber is completely disbonded. This shows that $G_{\ell 12}$, $G_{\ell 13}$ as well as $G_{\ell 23}$ are relatively insensitive to the disbonding of the center fractured fiber.

The thermal expansion coefficients are considered in Fig. 7. The lines representing the transverse thermal expansion coefficients are coincident, as to be expected. The disbonding conditions considered here produced a decrease in the transverse thermal expansion coefficients by 0.3 percent. This decrease is minimal and may be considered to be insignificant.

The line describing the change in the longitudinal thermal expansion coefficient is also displayed in Fig. 7. $\alpha_{\ell 11}$ increased by 20 percent when the center fiber is totally disbonded. Of all the material properties considered, $\alpha_{\ell 11}$ is the most sensitive to center fiber disbonding and is very significant.

High Temperature (1500 °F) Ply Properties with Center Fiber Disbonding

Figure 8 shows the degradation of longitudinal and transverse moduli. Since 11.1 percent of the effect of the fiber has been removed due to the total disbonding of the center fiber, a decrease of only a 7.3 percent is witnessed in $E_{\ell 11}$. This decrease is of the same magnitude as that observed for the room temperature $E_{\ell 11}$. The conclusion is that, the change in $E_{\ell 11}$ brought about by center fiber disbonding is significant.

Due to geometric effects, $E_{\ell 22}$ decreases by 2 percent when the center fiber is disbonded (Fig. 8). This decrease is due to the reduced effective cross-sectional area, and the subsequent reduced transverse stiffness of the composite, as resulting from the disbonding of the center fiber. This hole removes some of the stiffness from the model resulting in a lower transverse modulus. Note that this decrease is almost the same as the room temperature decrease in $E_{\ell 22}$ and $E_{\ell 33}$.

In Fig. 9 the Poisson's ratios of the composite are plotted. $\nu_{\ell 12}$ and $\nu_{\ell 23}$ decrease by approximately 1.5 percent when the center fiber is disbonded fully. When compared to the room temperature results, it is evident that there is a small increase in the change of $\nu_{\ell 12}$, and the change in $\nu_{\ell 23}$ is about the same. From these results it may be concluded that temperature has little effect on the rate of degradation of Poisson's ratios. $\nu_{\ell 12}$, $\nu_{\ell 13}$, $\nu_{\ell 23}$ and $\nu_{\ell 32}$ may all be considered to be relatively insensitive to center fiber disbonding.

$G_{\ell 12}$ degrades by almost 5 percent with the disbonding of the center fiber (Fig. 10). The change in $G_{\ell 12}$ at room temperature is 3 percent and at high temperature it is 5 percent when the center fiber is disbonded. $G_{\ell 23}$, at high temperature, has degraded by almost 3 percent when the center fiber has totally disbonded. $G_{\ell 12}$ and $G_{\ell 23}$ can all be said to be relatively insensitive to center fiber disbonding.

Figure 11 contains the plots that represent the changes in thermal expansion coefficients at high temperature as the center fiber is disbonded. $\alpha_{\ell 22}$ increased by less than 1 percent, an insignificant amount.

In figure 11, $\alpha_{\ell 11}$ shows an increase of 17.3 percent when the center fiber is completely disbonded which represents a decrease in effective fiber area of 11.1 percent. This change in $\alpha_{\ell 11}$ is significant and close to the percent change in $\alpha_{\ell 11}$ at room temperature.

Room Temperature Ply Properties with All Fibers Disbonding

The effect on the ply moduli of all the fibers disbonding is plotted in Fig. 12. The degradation of $E_{\ell 11}$ is now obviously nonlinear. $E_{\ell 11}$, with 100 percent fiber disbonding, has decreased by 78.2 percent and is lower than E_m. The cylindrical holes left by the disbonded fibers decrease the stiffness of the composite, much like a sponge. The composite can actually have a lower modulus than that of the matrix alone.

$E_{\ell 22}$ decreased by only 15 percent with 100 percent fiber disbonding (Fig. 12). The decrease in $E_{\ell 22}$ is due to the sponge effect.

In Fig. 13 $\nu_{\ell 12}$ increases until about 25 percent disbonding, then $\nu_{\ell 12}$ decreases gradually to 100 percent disbonding. This phenomenon will have to be examined in future work.

One hundred percent disbonding brought about a decrease in $\nu_{\ell 23}$ of 26.7 percent as shown in Fig. 13. The value at 100 percent disbonding is less than that of the matrix alone. This may be due to the spongy effect of the disbonded composite, where a significant percentage of the transverse displacements take place in the cylinders left by the disbonded fibers, resulting in less transverse strain.

Figure 14 represents the results of disbonding on the shear moduli at room temperature. Both $G_{\ell 12}$ and $G_{\ell 23}$ show an approximate degradation of 25 percent when the fibers are completely disbonded. As before, at 100 percent disbonding, these ply properties are lower in value than that of the matrix material alone, presumably due to the sponge effect discussed earlier.

Figure 15 shows the change in the composite's thermal expansion coefficients when disbonding is taken from 0 to 100 percent at room temperature. $\alpha_{\ell 11}$ increases drastically as the disbonding

increases. At 100 percent disbonding, $\alpha_{\ell 11}$ has increased by 557 percent. The value of $\alpha_{\ell 11}$ at 100 percent disbonding is virtually identical to that of the matrix alone.

The degradation of $\alpha_{\ell 22}$ is also depicted in Fig. 15. $\alpha_{\ell 22}$ degrades by only 14 percent when all fibers are completely disbonded. The significance in these results is that the final value for $\alpha_{\ell 22}$ and $\alpha_{\ell 33}$ is virtually equal to α_m. This would tend to imply that the sponge effect discussed earlier has little effect on thermal expansion.

It is significant to note that $\alpha_{\ell 11}$, $\alpha_{\ell 22}$, and $\alpha_{\ell 33}$ all approach α_m when the composite is approaching a quasi-monolithic state.

High Temperature (1500 °F) Ply Property With All Fibers Disbonding

Consider now high temperature (1500 °F) conditions while disbonding nine fibers. $E_{\ell 11}$ is nonlinear and degrades rapidly during initial disbonding but tends to stabilize as disbonding approaches 100 percent (Fig 16). This curve is similar in shape to that of room temperature $E_{\ell 11}$ except it is shifted down the ordinate. The total decrease in $E_{\ell 11}$ is 85.6 percent and its value at 100 percent disbonding is lower than that of the matrix alone. Again, this is probably due to the sponge effect. The transverse modulus $E_{\ell 22}$ degrades by 20.6 percent at 100 percent fiber disbond (Fig 16).

Figure 17 shows the effect of fiber disbonding on the Poison's ratios at high temperature for all fibers disbonding. As with the room temperature results, $\nu_{\ell 12}$ increases initially and then begins to decrease at about 25 percent disbonding. The total decrease in $\nu_{\ell 12}$, from 0 percent disbonding to 100 percent disbonding, is 9.1 percent. $\nu_{\ell 23}$ decreases linearly with fiber disbonding as seen in Fig. 17. These material properties decreased by 29.6 percent when 100 percent disbonding is reached.

Figure 18 shows a linear decrease in $G_{\ell 12}$ with fiber disbonding. $G_{\ell 12}$ decreased by 35.7 percent when the composite is at 100 percent disbonding. This is the same trend seen at room temperature. The degradation of $G_{\ell 23}$, as seen in Fig. 18, is slightly nonlinear both at high temperature and at room temperature (Fig. 14). $G_{\ell 23}$ shows a slight increase in slope after about 25 percent disbonding. The total decrease in $G_{\ell 23}$ is 34.2 percent at 100 percent disbond.

Figure 19 depicts the change in the composite's thermal expansion coefficients through the range of 0 to 100 percent disbonding at 1500 °F. As the percent disbond increased, a significant increase in $\alpha_{\ell 11}$ is evident. At 100 percent disbonding, $\alpha_{\ell 11}$ has increased by 799 percent and is virtually the same as $\alpha_{\ell 22}$ and $\alpha_{\ell 33}$ at 100 percent disbonding. The degradation in $\alpha_{\ell 22}$ appears to be minimal. The three thermal expansion coefficients approach the value of the matrix expansion coefficient at 100 percent fiber disbonding.

Conclusions

From the results of this analysis it can be seen that, in general, single fiber fracture and disbonding have little effect on most of the material properties. Of the material properties considered, the longitudinal thermal expansion coefficient $\alpha_{\ell 11}$ and the longitudinal modulus $E_{\ell 11}$ appear to be more sensitive to fiber disbonding. This sensitivity of $\alpha_{\ell 11}$ makes it a good indicator of the level of disbonding in a composite. If $\alpha_{\ell 11}$ is above predicted values, then the suspicion of the presence of disbonding of fractural fibers may be justified. The degree of disbonding may be approximated by comparing with the results shown here.

High temperature results indicate a shift in the value of the material properties while maintaining the same rate of degradation as in the room temperature results.

When all the fibers are fractured and disbonded, more significant changes in the material's ply properties are observed. The longitudinal modulus, $E_{\ell 11}$, and $\nu_{\ell 12}$ both show nonlinear degradation at these higher levels of fiber disbonding. Again the sensitivity of $\alpha_{\ell 11}$ to the disbonding of fracture of all fibers reinforces the idea that it is a good indicator of the degree of disbonding and fiber fracture in a composite.

This work has shown that for small amounts of partial bonding on fractured fibers, composite material properties are not significantly affected. However, when most of the fibers are fractured and disbonded, substantial degradation of the ply properties can be expected.

References

1. Caruso, J.J., "Application of Finite Element Substructuring to Composite Micromechanics," NASA TM-83729, 1984.

2. Caruso, J.J., and Chamis, C.C., "Superelement Methods Applications to Micromechanics of High Temperature Metal Matrix Composites," AIAA 29th Structures, Structural Dynamics, and Materials, Conference, Part 3, AIAA, 1988, pp. 1388-1400.

3. Gockel, M.A., ed., MSC/NASTRAN Handbook for Superelement Analysis: MSC/NASTRAN Version 61, The MacNeal-Schwendler Corporation, Los Angeles, 1982, p. 1.1-1.

4. Hopkins, D.A., and Chamis, C.C., "A Unique Set of Micromechanics Equations for High Temperature Metal Matrix Composites," NASA TM-87154, 1985.

TABLE I. - COMPOSITE MATERIAL PROPERTIES NO DISBONDING - ALL FIBERS LOADED P100-GRAPHITE/ COPPER

		Composite properties
$E_{\ell 11}$	psi	58.03×10^6
$E_{\ell 22}$	psi	7.19×10^6
$E_{\ell 33}$	psi	7.19×10^6
$G_{\ell 12}$	psi	3.36×10^6
$G_{\ell 23}$	psi	2.66×10^6
$G_{\ell 13}$	psi	3.36×10^6
$\nu_{\ell 12}$		0.291
$\nu_{\ell 23}$		0.246
$\alpha_{\ell 11}$	$\frac{in}{in\ °F}$	1.11×10^{-6}
$\alpha_{\ell 22}$	$\frac{in}{in\ °F}$	11.41×10^{-6}
$\alpha_{\ell 33}$	$\frac{in}{in\ °F}$	11.41×10^{-6}

TABLE II. - ROOM AND HIGH TEMPERATURE CONSTITUTIVE MATERIAL PROPERTIES P100-GRAPHITE/COPPER

		Room temperature		High temperature	
		Fiber	Matrix	Fiber	Matrix
E_{11}	psi	105.0×10^6	17.0×10^6	93.8×10^6	8.87×10^6
E_{22}	psi	0.90×10^6	17.0×10^6	0.904×10^6	8.87×10^6
E_{33}	psi	0.90×10^6	17.0×10^6	0.904×10^6	8.87×10^6
G_{12}	psi	1.10×10^6	6.54×10^6	0.982×10^6	3.41×10^6
G_{23}	psi	0.70×10^6	6.54×10^6	0.625×10^6	3.41×10^6
G_{13}	psi	1.10×10^6	6.54×10^6	0.982×10^6	3.41×10^6
ν_{12}		0.200	0.300	0.179	0.300
ν_{23}		0.250	0.300	0.223	0.300
ν_{13}		0.200	0.300	0.179	0.300
α_{11}	$\frac{in}{in\ °F}$	-0.90×10^{-6}	9.80×10^{-6}	-1.008×10^{-6}	19.55×10^{-6}
α_{22}	$\frac{in}{in\ °F}$	5.60×10^{-6}	9.80×10^{-6}	6.27×10^{-6}	19.55×10^{-6}
α_{33}	$\frac{in}{in\ °F}$	5.60×10^{-6}	9.80×10^{-6}	6.37×10^{-6}	19.55×10^{-6}

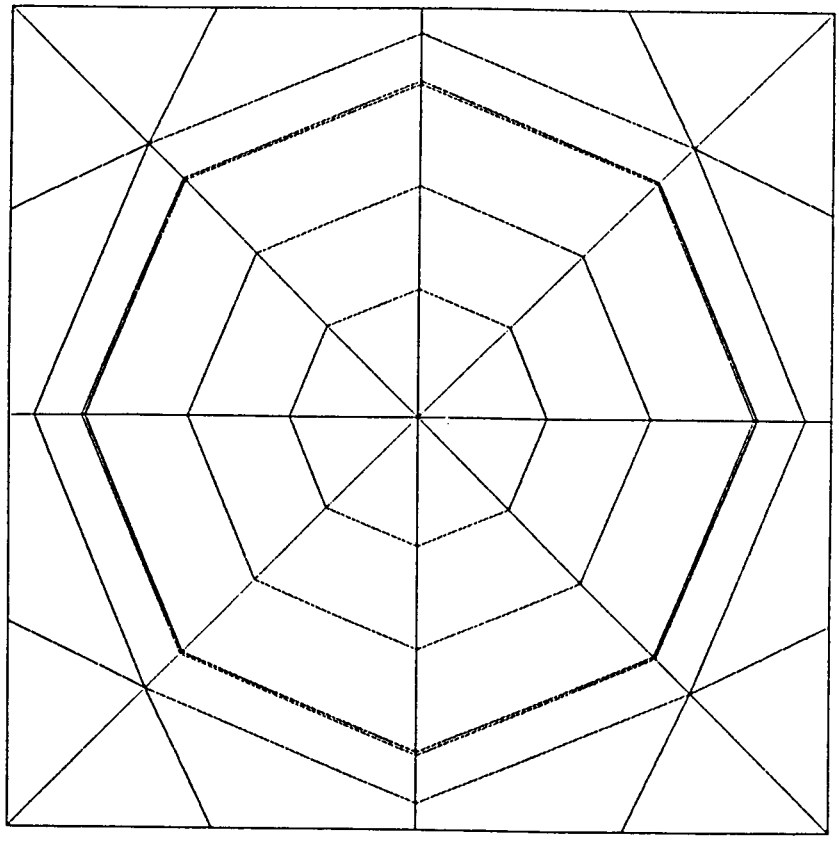

Figure 1. Finite element model - Unit cell

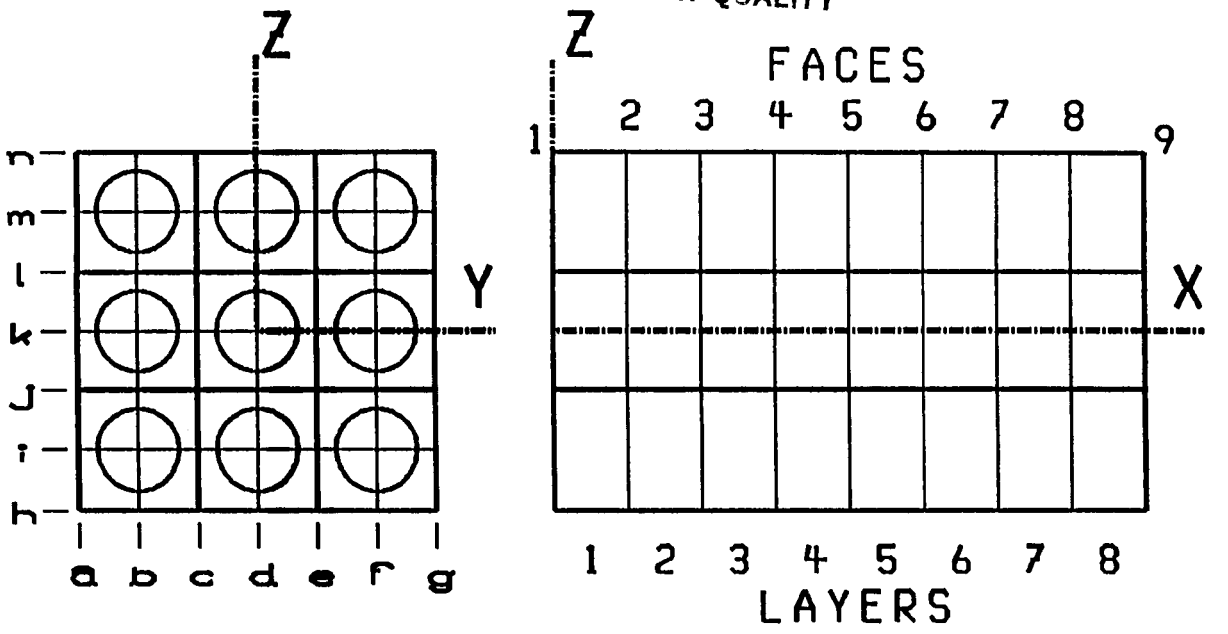

Figure 2. Representation of nine cell finite element mesh

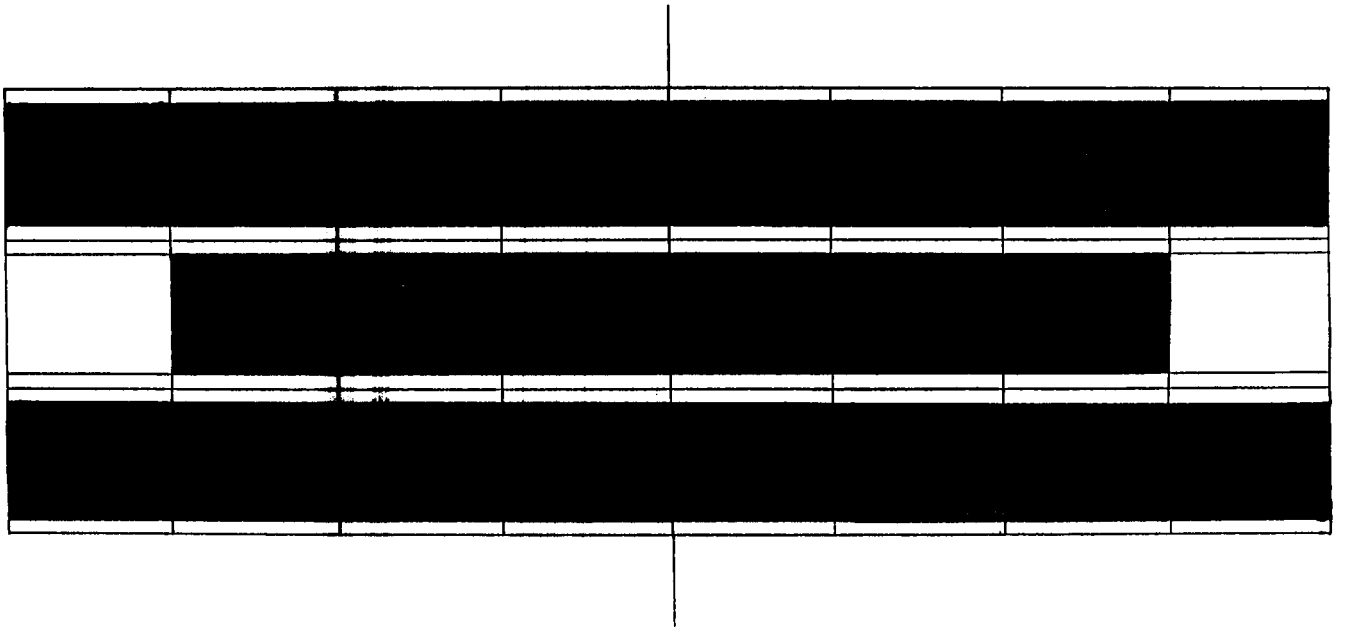

Plane
of
symmetry

Figure 3. Center fiber disbonding showing 2.78% disbonding

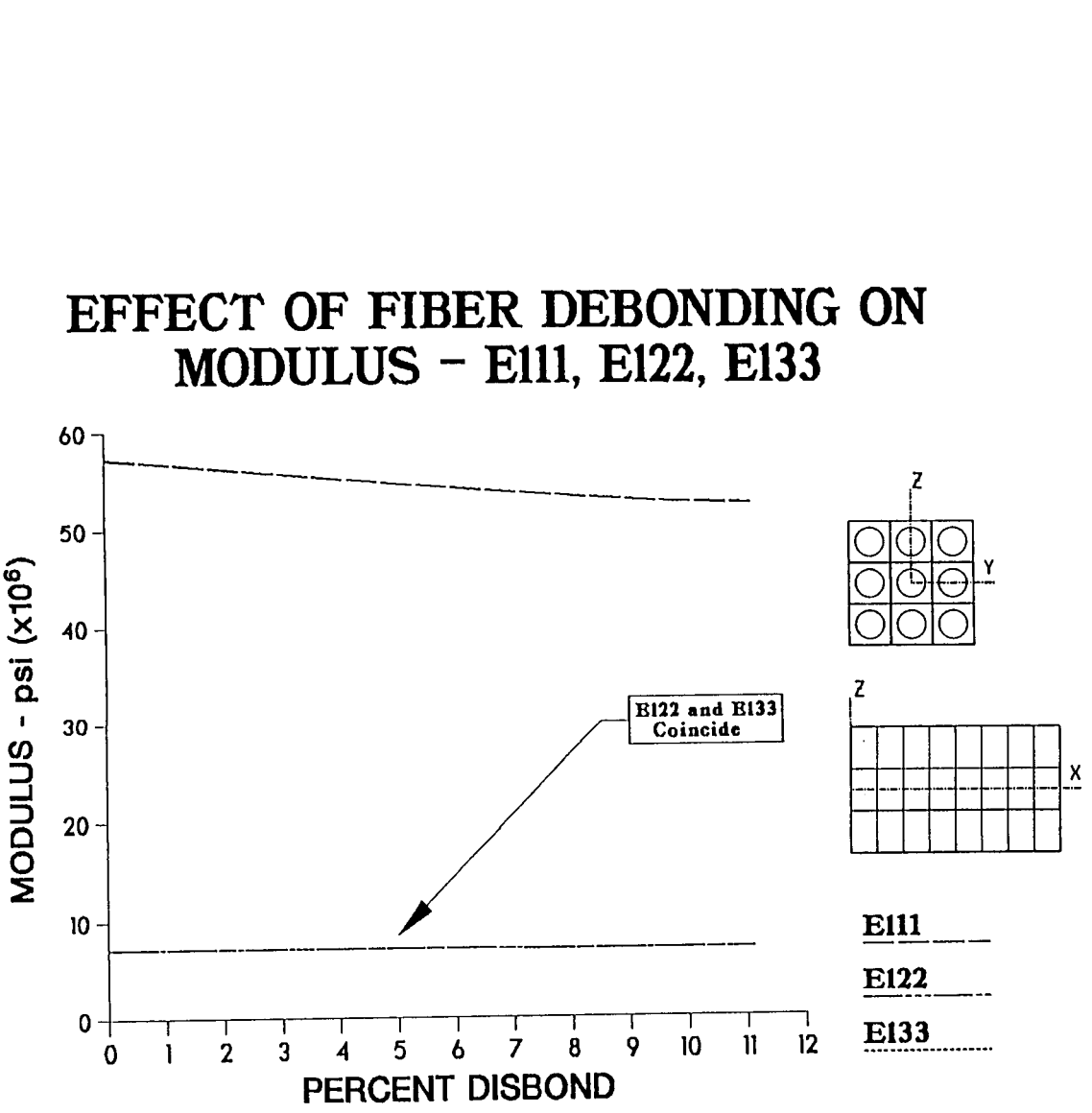

Figure 4. Effects of center fiber disbonding at room temperature on moduli

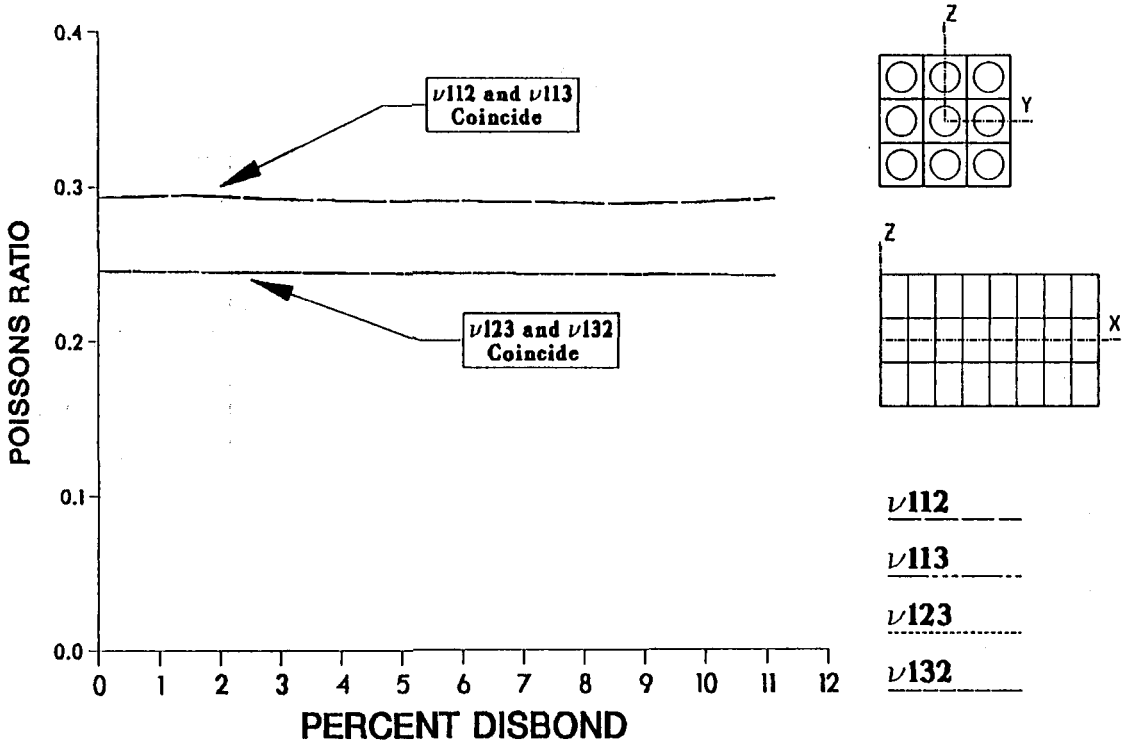

Figure 5. Effects of center fiber disbonding at room temperature on Poisson's ratio

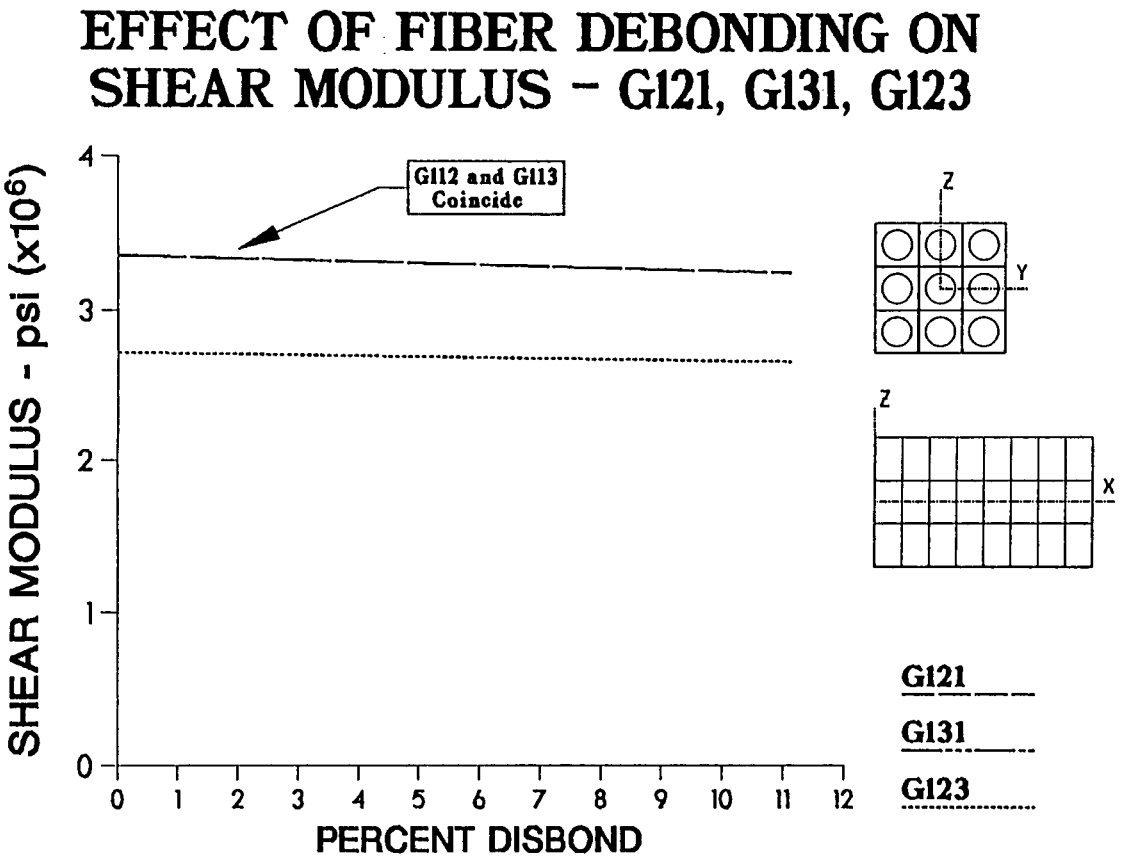

Figure 6. Effects of center fiber disbonding at room temperature on shear moduli

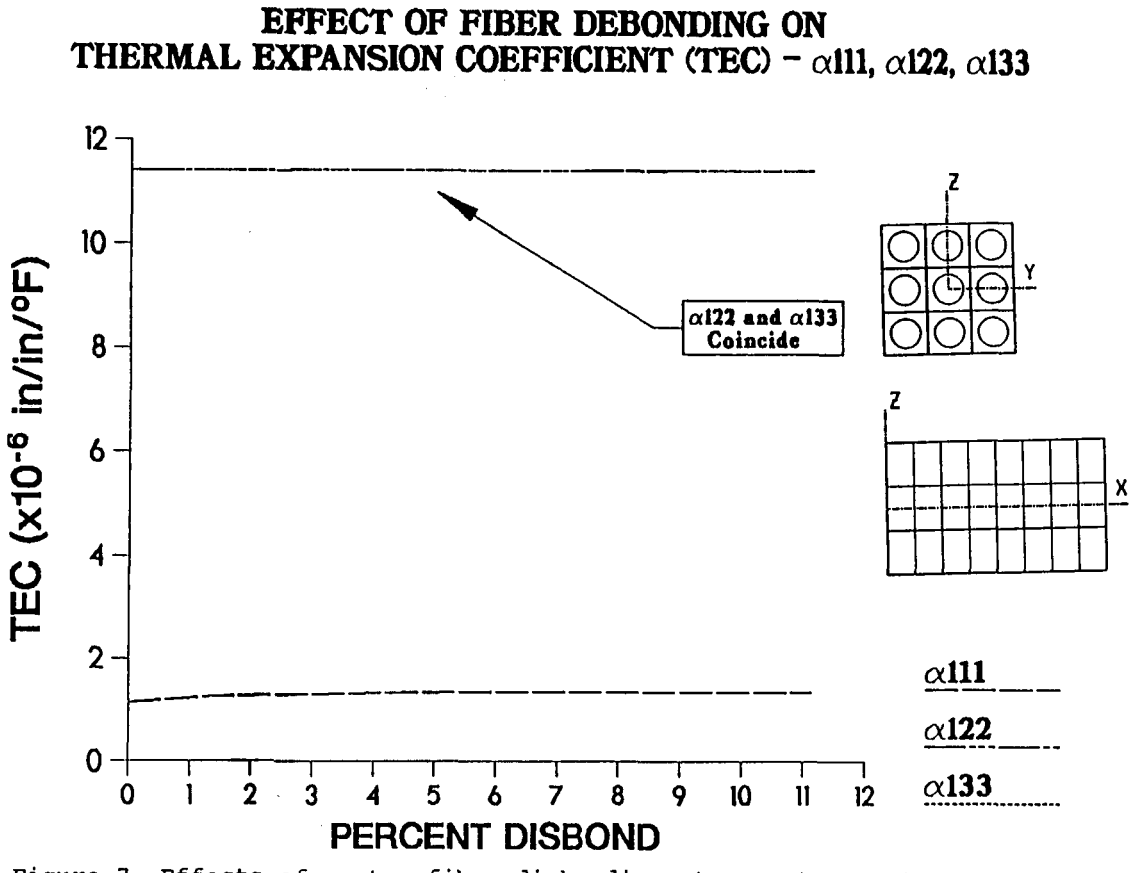

Figure 7. Effects of center fiber disbonding at room temperature on thermal expansion coefficients

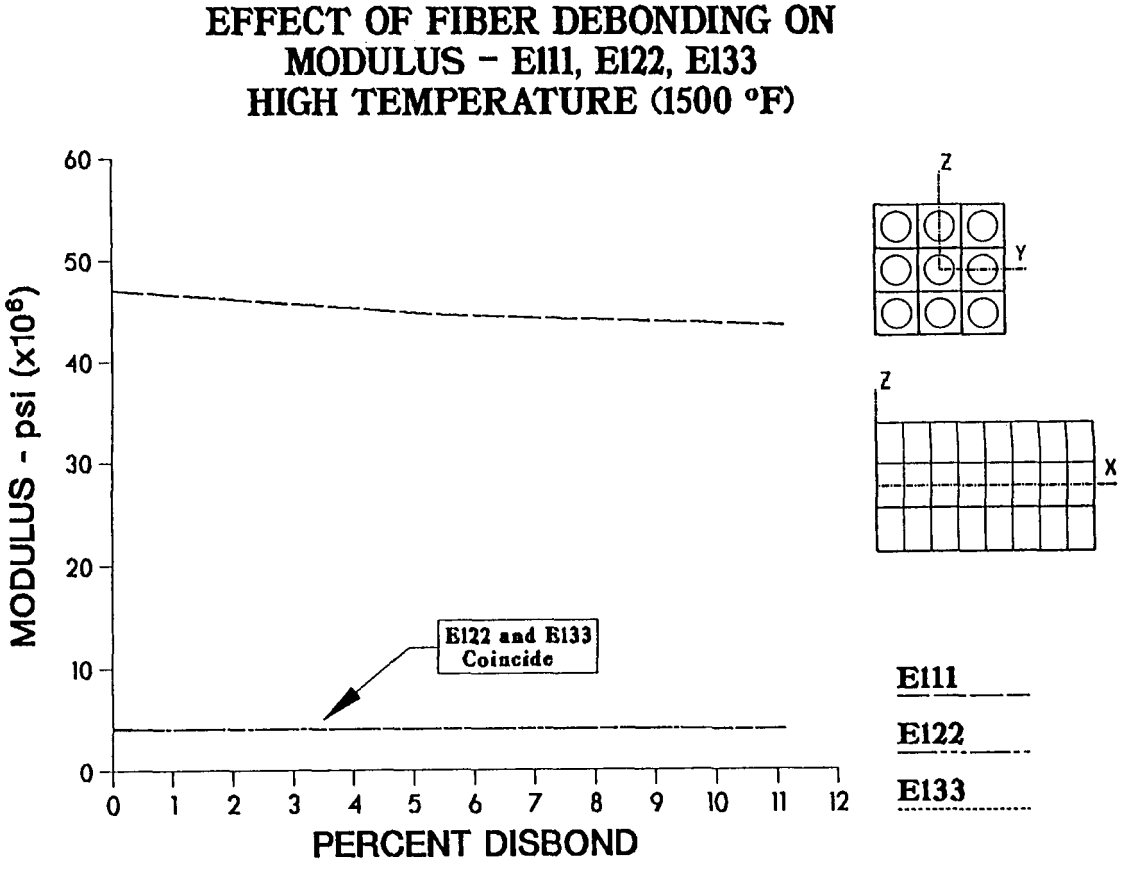

Figure 8. Effects of center fiber disbonding at high temperature on moduli

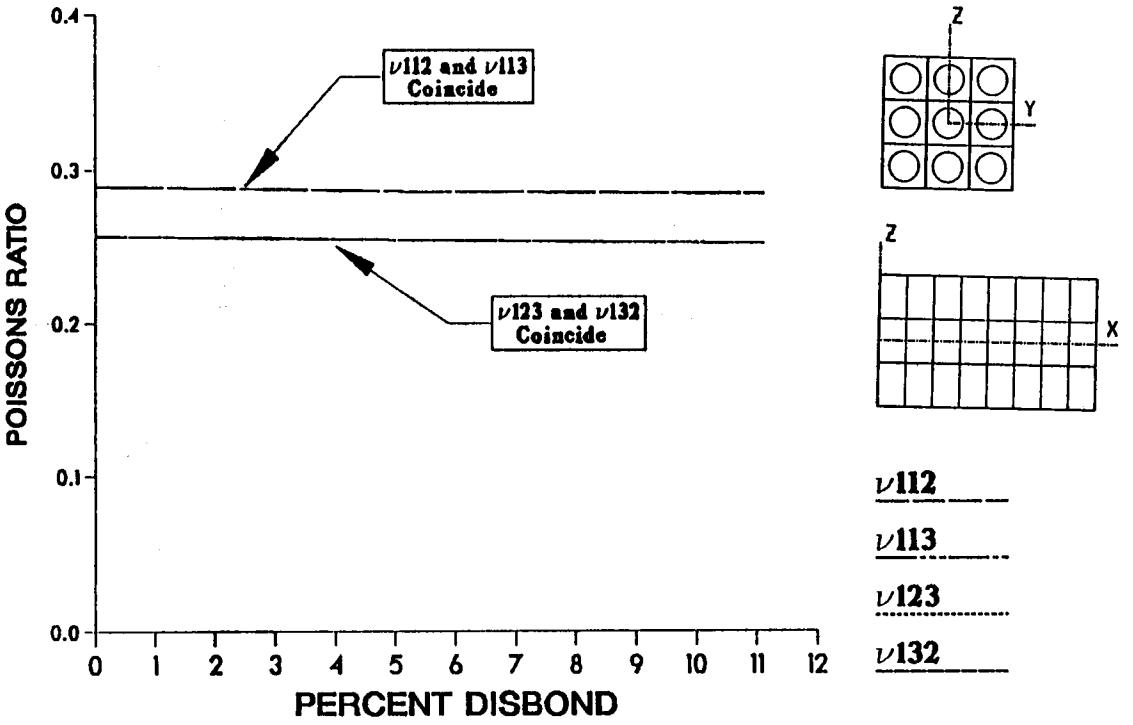

Figure 9. Effects of center fiber disbonding at high temperature on Poisson's ratio

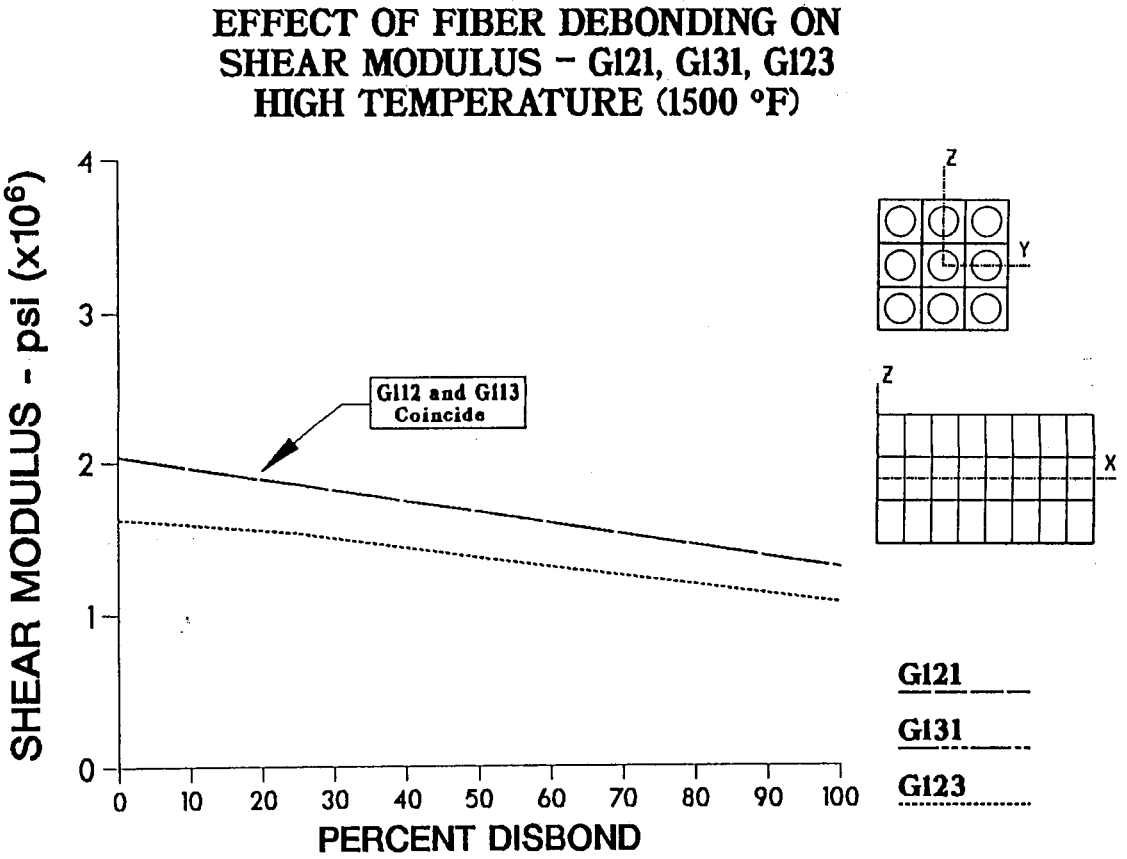

Figure 10. Effects of center fiber disbonding at high temperature on shear moduli

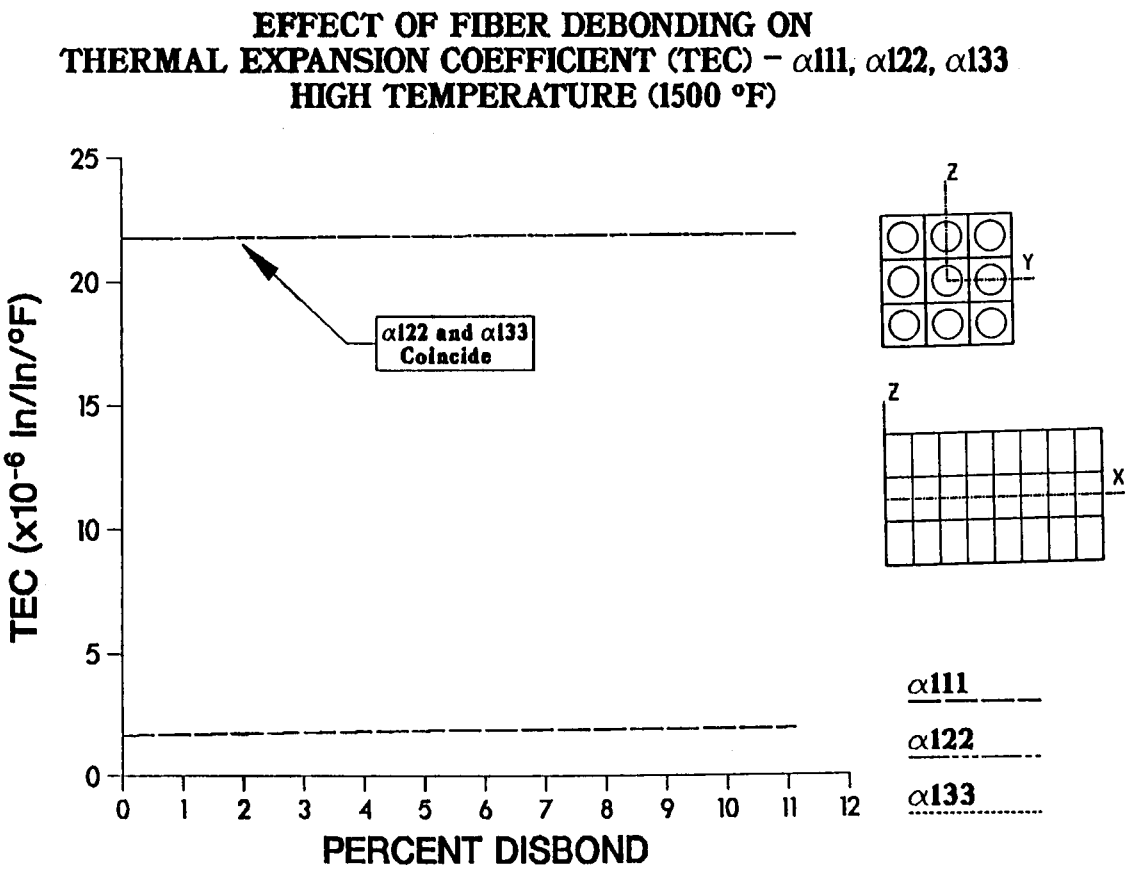

Figure 11. Effects of center fiber disbonding at high temperature on thermal expansion coefficients

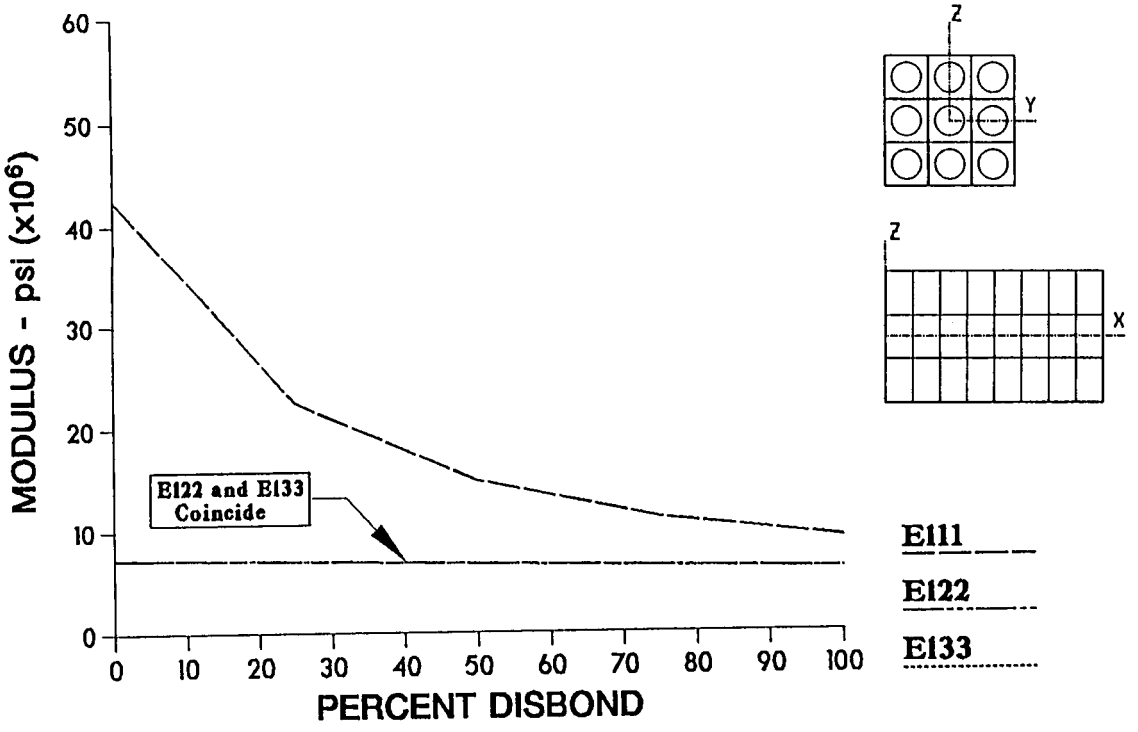

Figure 12. Effects of nine fiber disbonding at room temperature of moduli

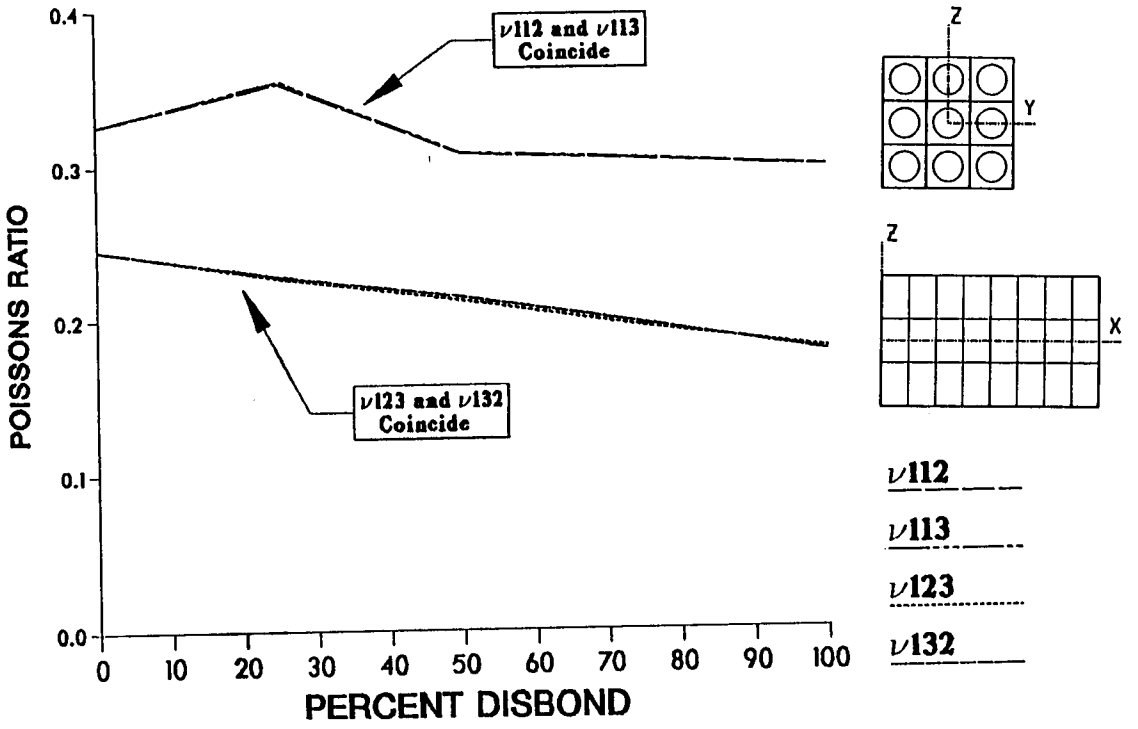

Figure 13. Effects of nine fiber disbonding at room temperature on Poisson's ratio

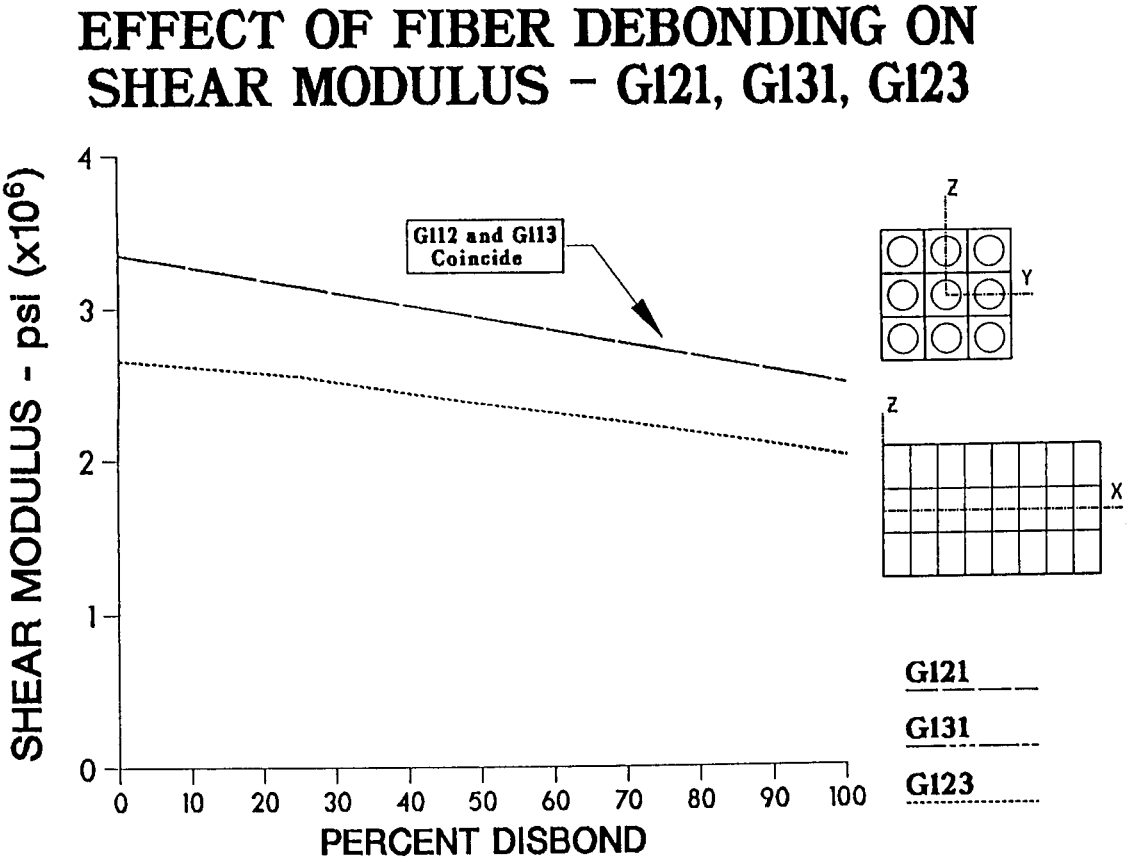

Figure 14. Effects of nine fiber disbonding at room temperature on shear moduli

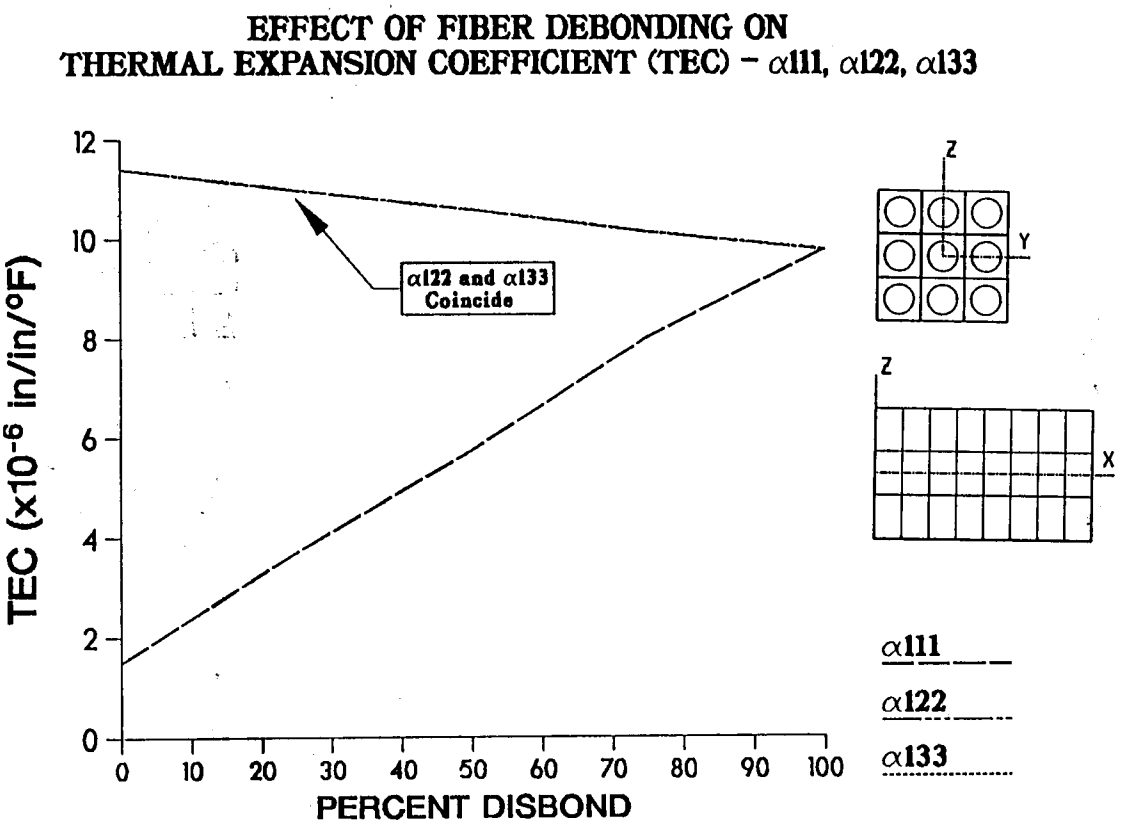

Figure 15. Effects of nine fiber disbonding at room temperature on thermal expansion coefficients

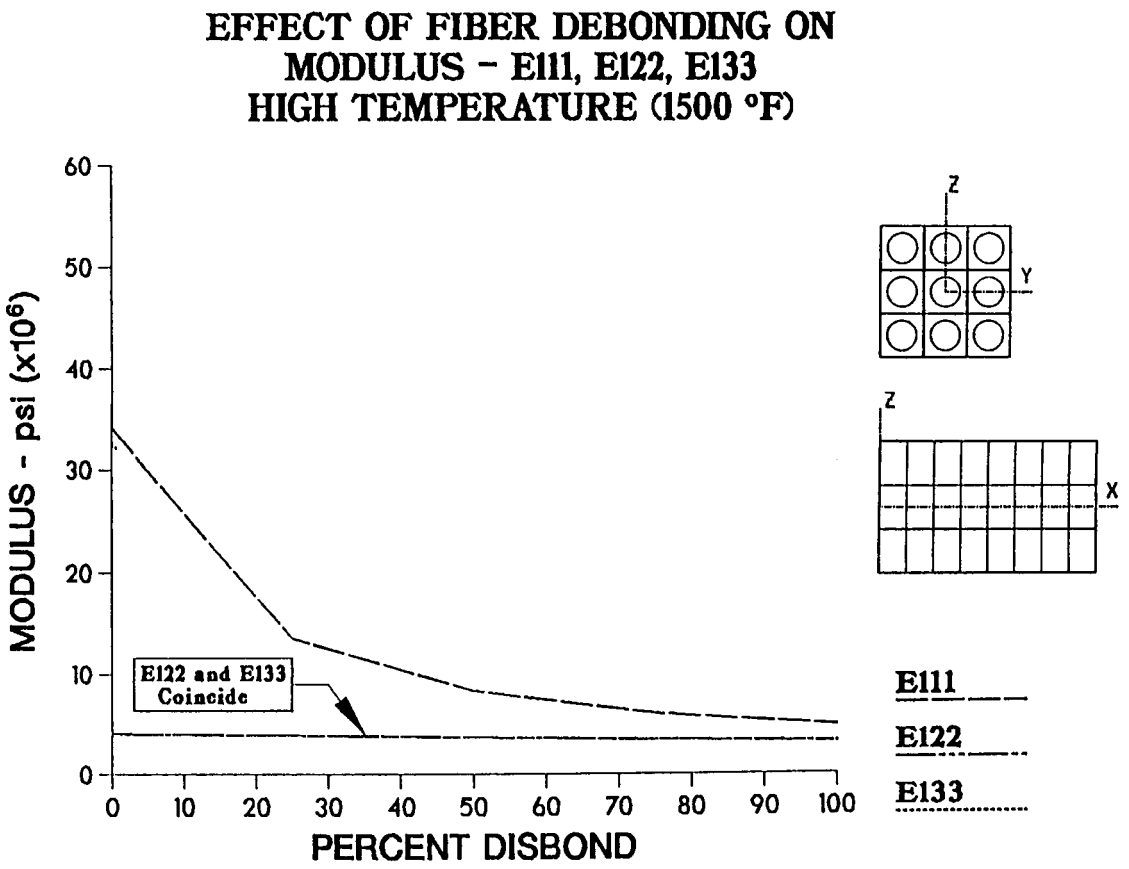

Figure 16. Effects of nine fiber disbonding at high temperature on moduli

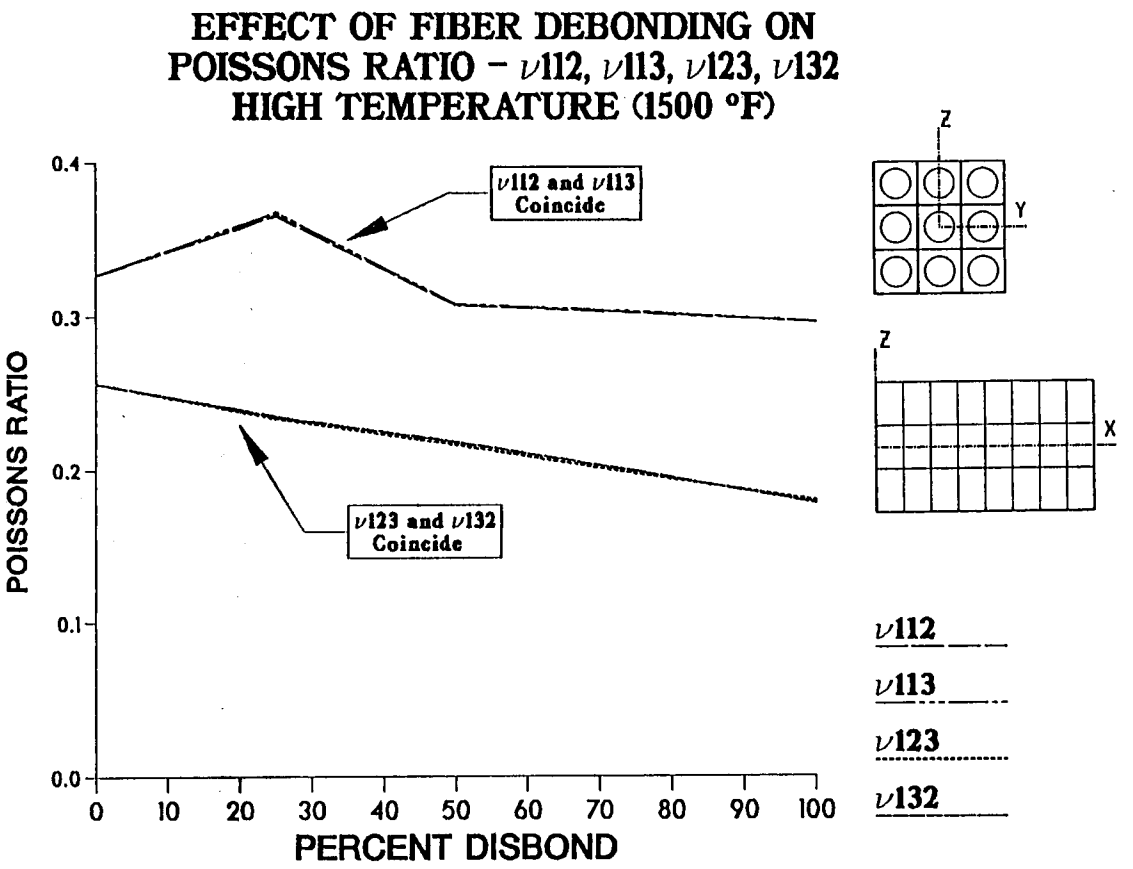

Figure 17. Effects of nine fiber disbonding at high temperature on Poisson's ratio

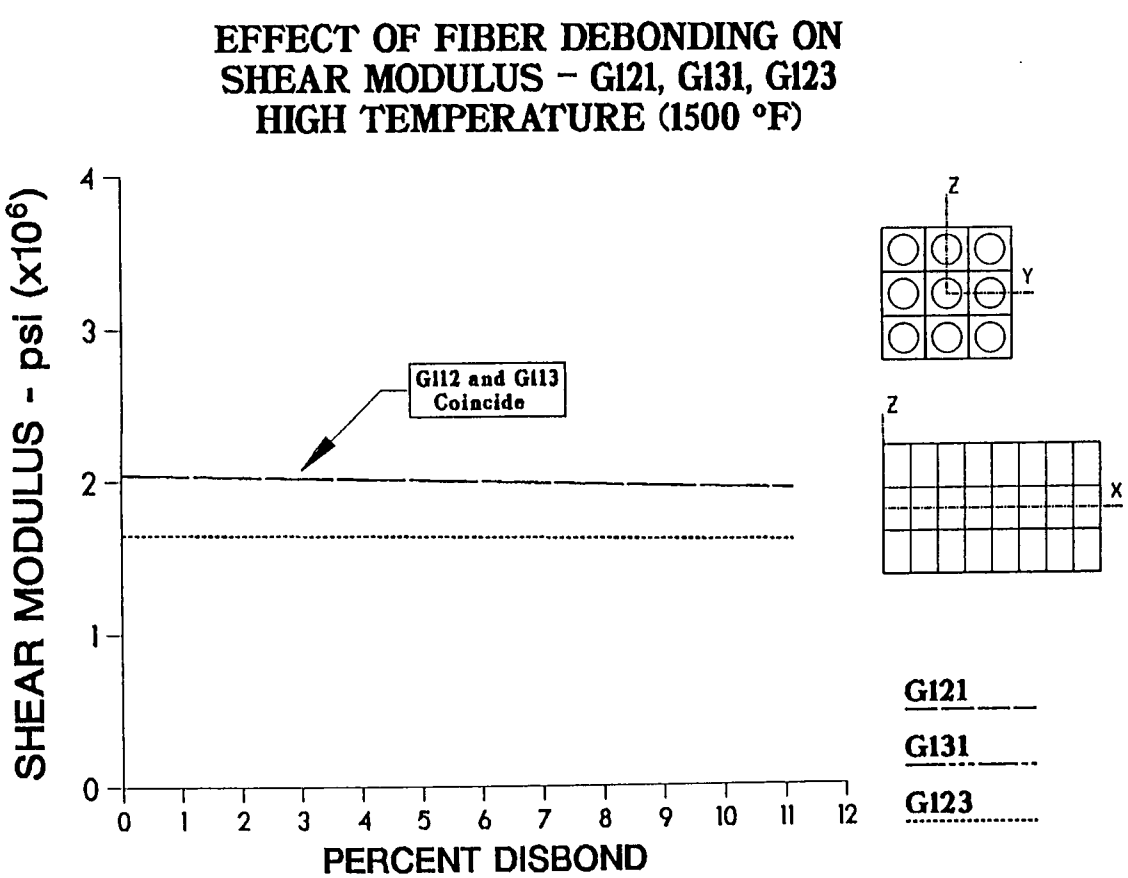

Figure 18. Effects of nine fiber disbonding at high temperature on shear moduli

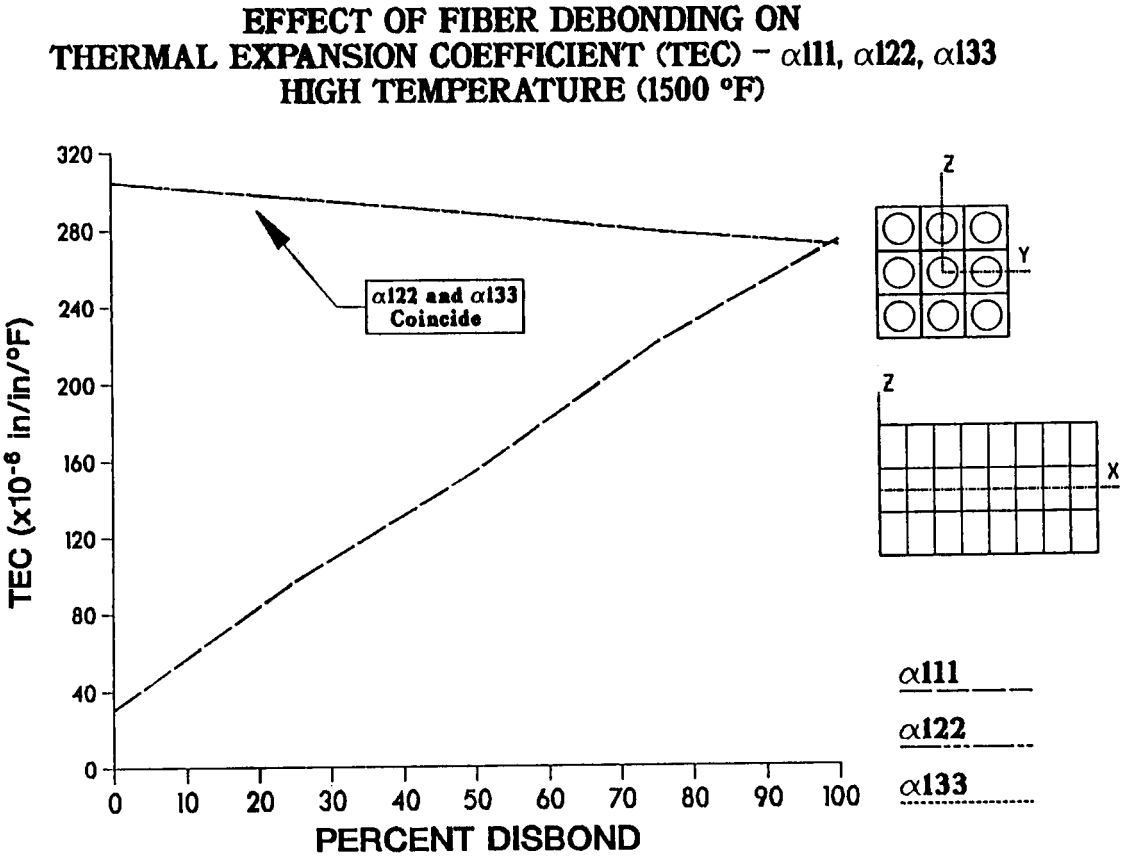

Figure 19. Effects of nine fiber disbonding at high temperature on thermal expansion coefficients

NASA
National Aeronautics and Space Administration

Report Documentation Page

1. Report No.	2. Government Accession No.	3. Recipient's Catalog No.
NASA TM-101482		

4. Title and Subtitle

Finite Element Applications to Explore the Effects of Partial Bonding on Metal Matrix Composite Properties

5. Report Date

6. Performing Organization Code

7. Author(s)

J.J. Caruso, D. Trowbridge, and C.C. Chamis

8. Performing Organization Report No.

E-4610

10. Work Unit No.

505-63-11

9. Performing Organization Name and Address

National Aeronautics and Space Administration
Lewis Research Center
Cleveland, Ohio 44135-3191

11. Contract or Grant No.

13. Type of Report and Period Covered

Technical Memorandum

12. Sponsoring Agency Name and Address

National Aeronautics and Space Administration
Washington, D.C. 20546-0001

14. Sponsoring Agency Code

15. Supplementary Notes

Prepared for the 30th Structures, Structural Dynamics and Materials Conference cosponsored by the AIAA, ASME, ASCE, AHS, and ACS, Mobile, Alabama, April 3-5, 1989. J.J. Caruso and C.C. Chamis, NASA Lewis Research Center; D. Trowbridge, The University of Akron, Akron, Ohio 44325.

16. Abstract

The mechanics of materials approach (definition of E, G, ν, and α) and the finite element method are used to explore the effects of partial bonding and fiber fracture on the behavior of high temperature metal matrix composites. Composite ply properties are calculated for various degrees of disbonding to evaluate the sensitivity of these properties to the presence of fiber/matrix disbonding and fiber fracture. The mechanics of materials approach allows for the determination of the basic ply material properties needed for design/analysis of composites. The finite element method provides the necessary structural response (forces and displacements) for the mechanics of materials equations. Results show that disbonding of fractured fibers affect only E_{111} and α_{111} significantly.

17. Key Words (Suggested by Author(s))	18. Distribution Statement
Partial bonding; Fiber fracture; Square array; Composite properties; Superelement; Finite element; P100/copper	Unclassified – Unlimited Subject Category 24

19. Security Classif. (of this report)	20. Security Classif. (of this page)	21. No of pages	22. Price*
Unclassified	Unclassified	24	A03

*For sale by the National Technical Information Service, Springfield, Virginia 22161